# NANOINDENTATION-INDUCED PHASE TRANSFORMATIONS IN HgCdTe EPITAXIAL HETEROSTRUCTURES

F. SIZOV, A. RICHTER[1], YE. BILEVYCH, Z. TSYBRII, K. KUBICA[1], R. RIES[1], YU. SIDOROV[2]

UDC 621.382, 539.32


**V. Lashkarev Institute of Semiconductor Physics, Nat. Acad. Sci. of Ukraine**
*(41, Nauky Prosp., Kyiv 03028, Ukraine),*

[2]**University of Applied Science**
*(1, Bahnhofstrasse, Wildau 15745, Germany),*

[3]**Institute of Semiconductor Physics, Acad. Sci., Russia**
*(13, Lavrent'eva Prosp., Novosibirsk 630090, Russia)*

Mercury-cadmium-telluride (MCT) epitaxial heterostructures grown by molecular beam epitaxy (MBE) and liquid phase epitaxy (LPE) were subjected to nanoindentation for revealing possible phase transitions in the vicinity of heteroboundaries. The nanoindentation load — displacement curves of the lattice mismatched MCT based heterostructures grown by MBE on GaAs substrates with ZnTe/CdTe buffer layers displayed the characteristic "elbow" behavior in the unloading part of the curves. In the lattice matched MCT heterostructures grown by LPE on the ZnCdTe substrate, the more pronounced bending of similar curves and the evident "pop-out" effect, which presumably are connected with phase structural transformations at these heterostructures heteroboundaries, are revealed.

## 1. Introduction

MCT is an important material for its applications in microphotoelectronic infrared (IR) devices in imaging arrays. As a rule, in many device applications, $Hg_{1-x}Cd_xTe$ ($x \approx 0.2$) epilayers are deposited on suitable substrates with same lattice constant, which is usually the $Cd_{1-y}Zn_yTe$ substrate, to minimize misfit dislocation defects in MCT layers. For MCT solid solutions with $x \approx 0.2$, the $Cd_{1-y}Zn_yTe$ compositions with $y \approx 0.04$ are fairly good matched to the MCT lattice [1].

Considerable efforts are applied up to now to grow large-area epitaxial layers on the alternative (not CdTe or $Cd_{1-y}Zn_yTe$) substrates. Among these substrates are used, e.g., GaAs or Si wafers [2—5]. In these regards, considerable efforts has been applied to prove the stability of MCT layers because of a large difference in the lattice constants of substrates and layers. Fairly good focal plane array characteristics were obtained in MCT heterostructure multielement arrays on GaAs substrates [6].

MBE procedure was used to grow large-area MCT layers on 2- or 3-inch (013) GaAs substrates with an intermediate ZnTe/CdTe buffer layer [7]. The layers in heteroepitaxial HgCdTe/CdTe/ZnTe/GaAs structures are not lattice-matched because of the large differences of the GaAs, ZnTe, CdTe, and HgCdTe lattice constants ($a_0$ (GaAs) = 5.653 Å, $a_0$(ZnTe) = 6.103 Å, and $a_0$(CdTe) = 6.482 Å, $a_0(Hg_{1-x}Cd_xTe$, $x$= 0.2) = 6.443 Å). These materials under normal conditions crystallize in $F\bar{4}3m$ lattice ($T_d$) (the zinc blende type structure of the lattice). Under pressure conditions, the structural phase transitions zinc blende (ZB) → cinnabar → sodium chloride (NaCl) → orthorhombic ($C_{mcm}$) occur in all of these semiconductors [8—11], except ZnTe that appears not possessing the NaCl structure at ambient temperature [12]. HgTe also a little differs from the sequence observed for other tellurides, as the "hidden" intermediate ZB → $C_{2221}$ → cinnabar symmetry transitions are observed in it [13].

The elastic or inelastic deformations of these materials can play an important role for a possible change in the properties of heterostructures near the boundaries, because of very different lattice constants compared with that one for GaAs, and also due to different temperature expansion coefficient dependences. This is owing to the natural tendency of strained heteroepitaxial layers to spontaneously form dislocation-free islands after the formation of uniform, but stressed, wetting layers. Strain energy relaxation is possible within the islands due to their lateral expansion (or compression) in the directions of the free side faces of the islands. A large point mechanical loading can change the equilibrium state in the stressed layers near the boundary which will cause a structural transformation near the critical boundary.

Nanoindentation is a relatively new technique designed to measure the mechanical properties of materials on the nanoscale [14, 15]. There exists a broad range of investigations implementing nanoindentation to different materials [16, 17].

The unloading curve is commonly regarded as purely elastic, apart from situations with strong viscosity, as found with polymers, or in the case of phase transformations that occur, e.g., in Si [17]. For the reason of simple separation of plasticity and elasticity, the unloading curve is used as the main source of information in the data analysis based on the Oliver—Pharr approach [14]. The loading curve — though containing, however, a lot of not easily accessible information — is commonly not used for the indentation experiment analysis.

Depth-sensing nanoindentation can provide important information about the mechanical properties even in the case of well-studied semiconductor materials (e.g., Si). It has been established that hardness of silicon at room temperature is controlled by the phase transformation pressure. Information on the phase transformation in the surface layer of silicon upon contact interaction is very important for understanding the mechanisms of wear and contact damage that occurs in many industrial processes [17].

Experimental values of the phase transformation may be assessed through the depth-sensing nanoindentation technique, which allows the high-resolution *in situ* monitoring of the indenter displacement as a function of the applied load. During the nanoindentation procedure controlled, e.g. by scanning force microscopy (SFM), the depth-sensing indentation load $F$ and the penetration depth $h_p$ are recorded simultaneously. Hardness $H$ and elastic modulus $E$ are inferred from the resulting load-depth curve $F(h)$. Changes in mechanical properties during a phase transition may be revealed as characteristic events in the load-displacement curve. For the elastoplastic materials, load (unload)-displacement curves have no peculiarities but, in the case of formation of a new phase under the (nano)indenter, may result in the yield step ("pop-in") or a change in the slope ("elbow") of the loading curve; a sudden displacement discontinuity ("pop-out") or an elbow in the unloading curve may be indicative of the transition [17].

MCT solid solutions and MCT-based heterojunctions are widely used in IR technologies [1, 3]. They are rather soft semiconductors and, at the same time, are brittle. Nanoindentation testing is, perhaps, the only one technique that allows a high degree of inelastic deformation without total sample destruction. The pressures attainable in nanoindentation experiments can be much higher compared to those during the uniaxial deformation. Recently an attempt to reveal the effects of Zn addition and thermal annealing on yield phenomena in CdTe and CdZnTe (CZT) single crystals was undertaken by nanoindentation [18].

The present investigations aimed to reveal, by nanoindentation experiments, the possible mechanical properties changes on the nanoscale of MCT-based heterostructures on lattice matched and mismatched substrates causing the tension of different layers in relatively thin MCT epitaxial layers.

## 2. Experiment

Nanoindentation experiments were performed with a HYSITRON Triboscope attached to a Nanoscope IV multimode scanning force microscope of Digital Instruments. The principal device of the Triboscope is an electrostatic transducer — a three-plate capacitor, the mid-plate of which is carrying the indentation tip mounted to a stylus. Application of a DC-voltage up to 600 V results in an electrostatic force (the maximum load depending on the capacitor plate spacing and area is at most 6.3 mN) that drives the diamond tip at the sample. The change in the capacitance is simultaneously recorded as a measure of penetration depth. The primary data (voltage $U$, capacitance change $\Delta C$) are converted into load $F$ and depth $h$, resulting in an $F(h)$-curve. After the complete unloading, the impression area can be scanned with the same tip. The stress distribution under indentation is largely affected by the indenter tip geometry, which is a vital factor in determining the boundary conditions for the field [17].

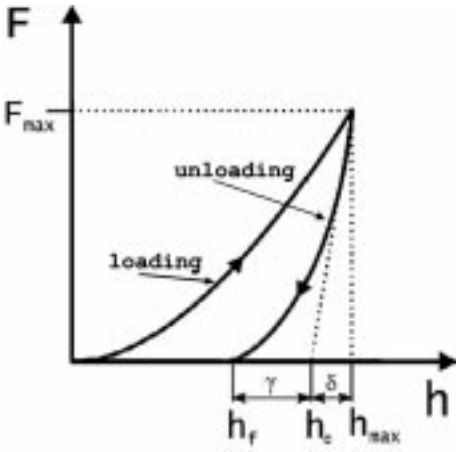


Fig. 1. Illustration of the parameters which can be extracted from loading-unloading dependences in nanoindentation experiments

A three-sided 90° pyramidal diamond tip was used for the indentation procedure. By these methods, the following parameters can be obtained (see also Fig. 1): maximum indentation depth $h_{\max}$, penetration depth $h_p$, depth of the remaining expression after complete unloading $h_t$, maximal applied force $F_{\max}$, nanohardness $H_N$, and Young's modulus $E_r$. The depth $h_c$ is the penetration depth, at which the cross section area $A_c$ is taken to calculate the hardness and Young's modulus. Here, the measurements were repeated 5—10 times, and the average values of data were calculated.

The key quantities to determine, namely the mechanical properties, are defined as follows. The maximum indentation depth $h_{\max}$ includes the elastic and plastic deformation. The depth, at which the applied forces becomes zero under unloading, is called $h_f$. The depth $h_c$ is the penetration depth at which the cross section area $A_c$ is taken to calculate hardness and Young's modulus. The nanohardness of the sample $H_N$ is determined using [14, 19]

$$H_N = \frac{F_{\max}}{A_c h_c}, \tag{1}$$

where $F_{\max}$ is the maximum applied load and $A_c$ is the cross-sectional area corresponding to the depth $h_c$. The determination of the contact depth $h_c$ is given by

$$h_c = h_{\max} - 0.75\frac{F_{\max}}{S}, \tag{2}$$

where $S$ is the contact stiffness

$$S = \frac{dF}{dh}, \tag{3}$$

with $dF/dh$ being the slope of the unloading curve at the initial point of unloading. The reduced Young's modulus $E_r$ is a measure of the elastic properties of the tip-sample system and can be calculated from the load-depth curves according to the formula

$$E_r = \frac{1}{2}\sqrt{\frac{\pi}{A_c h_c}}\frac{dF}{dh}. \tag{4}$$

For elastically deformable indenters, the reduced modulus $E_{\rm r}$ can be generalized and is defined as

$$\frac{1}{E_r} = \frac{1-\nu_s^2}{E_s} + \frac{1-\nu_t^2}{E_t}, \tag{5}$$

where $E_s$ and $\nu_s$ stand for Young's modulus and Poisson ratio of the sample, respectively, and $E_t$ and $\nu_t$ stand for Young's modulus and Poisson ratio of the indenter tip, respectively.

Since $E_t$ is much higher than $E_s$, the value of $E_r$ will hardly differ from $E_s$ for soft materials like MCT or some other II-VI compounds.

All experiments were carried out at room temperature in air atmosphere.

## 3. Samples

MCT heteroepitaxial layers for multielement photodiode arrays were grown by the MBE technology on (013) GaAs substrates with ZnTe/CdTe buffer layers [4, 6, 7] and had cutoff wavelength $\lambda_{\rm co}$ from 10.5 to 12.0 $\mu$m ($\pm$ 0.15 $\mu$m) at $T$ = 78 K in dependence on the growth conditions. MCT layers and GaAs substrates are different with lattice constants and have different thermal expansion coefficients ($\alpha_{\rm l} = 4.6{\times}10^{-6}$ K$^{-1}$ for $Hg_{0.8}Cd_{0.2}Te$, and $\alpha_{\rm l} = 5.3{\times}10^{-6}$ K$^{-1}$ for GaAs). The growth temperature was in the region $T \approx 180 \div 190$ °C for the HgCdTe layers and within $T = 240 \div 300$ °C for ZnTe/CdTe buffer layers. During the growth process, the composition of the layer was controlled by a built-in ellipsometer. The composition non-uniformity over 1 cm$^2$ area was not more than $\Delta x = \pm 0.001$. The as-grown layers had $n$-type conductivity (electron concentration $n_{77} \approx 2{\times}10^{15}$ cm$^{-3}$, electron mobility $\mu_{77} \approx 10^5$ cm$^2$/(V·s)). The following annealing was necessary to convert the $n$-type conductivity of the obtained layers into the $p$-type to manufacture $n^+ - p$-photodiodes by $B^+$ implantation. After the annealing procedure, the MBE MCT layers had hole concentrations about $p_{78} \approx (3 \div 10){\times}10^{15}$ cm$^{-3}$ with carrier mobility in the range of $\mu_{78} \approx 350 \div 400$ cm$^2$/(V·s). The dislocation densities in the material for those IR photodetectors were about $10^5$ cm$^{-2}$.

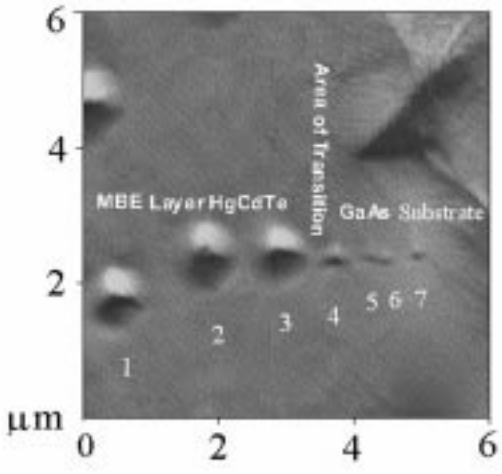


Fig. 2. SFM image of the nanoindentor impression for HgCdTe/CdTe/ZnTe/GaAs MBE layer near the heterostructure boundary

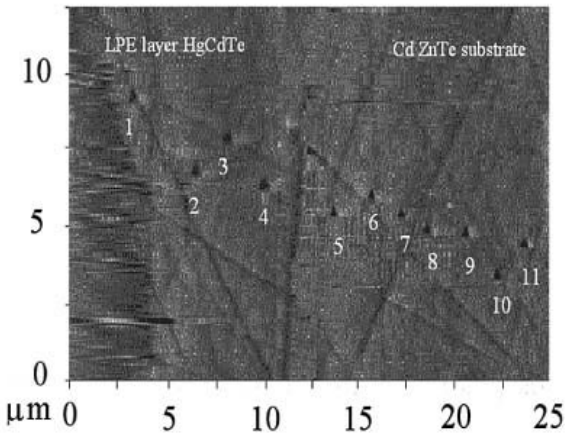


Fig. 3. SFM image of the nanoindentor impression for CdTe/HgCdTe LPE layer near the heterostructure boundary

The total thickness of the MBE structures investigated was within 10 to 12 $\mu$m. The thickness of ZnTe layers in different heterostructures was about 300 Å — 0.5 $\mu$m and the thickness of CdTe layers was within several microns. To decrease the influence of surface recombination HgCdTe layers were grown with $x$ increasing to the surface [20]. The layers have special wide gap regions of $d \approx 0.5$ $\mu$m thick with composition $x \approx 0.55$ near the surface, while the interior part of the layers was within $x \approx 0.21 \div 0.22$ in dependence of the growth conditions. Close to the buffer layer, the Cd content is also increasing and a potential barrier can be formed in some cases between the buffer and the photosensitive layer.

Also the HgCdTe/CdZnTe lattice matched heterostructures were grown by the LPE method. MCT epitaxial layers were grown on (111) CdZnTe single crystal substrates at $T \approx 500$ °C. MCT layers and CdZnTe substrates have similar lattice expansion coefficients. The thickness of these epitaxial layers was within 8—25 $\mu$m.

They were grown on $Cd_{1-y}Zn_yTe$ substrates with chemical composition $y \approx 0.04 \pm 0.02$. In the case of $y = 0.04$, the lattice constants of MCT layers with $x = 0.215$ coincide. The dislocation densities in the LPE layers were about $2{\times}10^4$ cm$^{-2}$. The LPE layers had hole concentrations about $p_{78} \approx (5 \div 20){\times}10^{15}$ cm$^{-3}$ with carrier mobility in the range of $\mu_{78} \approx 400 \div 500$ cm$^2$/(V·s).

## 4. Results and Discussion

To investigate the loading-unloading dependences at heterostructure boundaries the samples were clevaged or mechanically polished across the surface growth. In Figs. 2 and 3, we show the SFM image of MBE- and LPE-grown heterostructure cross-sections, respectively. Clearly is seen the difference area of the nanoindentor impression in dependence of its position near the heterostructure boundary for the MBE-grown structure, since the MCT is more soft than other materials of heterostructures.

The sizes of impressions (Fig. 3) are rather similar for different parts of LPE grown structure cross sections, which is an evidence of the rather similar hardnesses of HgCdTe and CdZnTe solid solutions.

In Figs. 4 and 5, we show the corresponding loading (unloading)-displacement (force-depth) dependences. Evidently, there exist the differences between the unloading-displacement dependences taken in different parts near the heterostructure border for both cases. Near the, or at GaAs/ZnTe/CdTe heterointerface (point 4) and at the HgCdTe layer (point 1), the "elbow" effect (Fig. 4) is clearly seen, which can be associated with phase transformations. The pop-out or elbow effect is absent for the points out of the border at the GaAs substrate (points 6) under experimental loading. The pronounced "elbow" effects and even pop-out effects (a sudden change of force-depth dependences) for both unloading curves are represented in Fig. 5, as a consequence of the phase transformation in HgCdTe

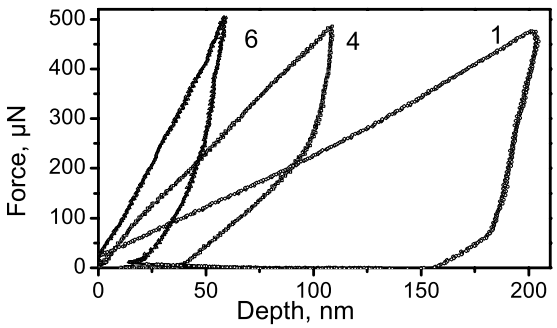


Fig. 4. Force/depth curves for nanohardness measurements in MBE heterostructures. Numbers above the curves correspond to numbers of nanoindentor impression points in Fig. 2

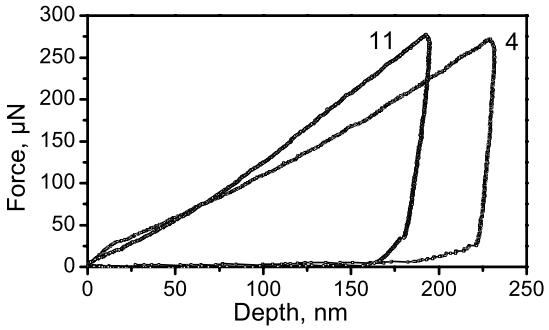


Fig. 5. Force/depth curves for nanohardness measurements in LPE heterostructures. Numbers above the curves correspond to numbers of nanoindentor impression points in Fig. 3

and CdZnTe epitaxial layers. Such phase transformations were revealed by other "macroscopic" methods [8—10, 21].

The average values of nanohardness and Young's modulus were calculated by using formulas (1) and (4), respectively. They are shown in Tables 1 and 2.

It is interesting to note that, despite the "elbow" and "pop-out" effects observed, which are presumably connected with phase transformations in the vicinity of the heterostructure boundaries, no influence of them on electrical and photoelectrical properties was observed.

**T a b l e 1. Elastic modulus and nanohardness of heterostructures HgCdTe/CdTe/ZnTe/GaAs grown by MBE methods (the number of points corresponds to numbers of the nanoindentor impression in Fig. 4)**

| Point number | $E_r$ (GPa) | $H$ (GPa) |
|---|---|---|
| 1 | 31.2 | 1.6 |
| 2 | 40.1 | 1.8 |
| 3 | 55.7 | 1.5 |
| 4 | 35.2 | 4.5 |
| 5 | 113.2 | 7.9 |
| 6 | 112.5 | 10.3 |
| 7 | 97.6 | 10.8 |

**T a b l e 2. Elastic modulus and nanohardness of heterostructures HgCdTe/CdZnTe grown by LPE methods (the number of points corresponds to numbers of nanoindentor impression in Fig. 5)**

| Point number | $E_r$ (GPa) | $H$ (GPa) |
|---|---|---|
| 1 | 48.7 | 1.7 |
| 2 | 43.4 | 1.3 |
| 3 | 65.5 | 1.4 |
| 4 | 74.7 | 1.5 |
| 5 | 43.6 | 2.0 |
| 6 | 57.2 | 2.1 |
| 7 | 53.9 | 2.1 |
| 8 | 59.5 | 2.8 |
| 9 | 66.9 | 2.4 |
| 10 | 67.5 | 2.5 |
| 11 | 73.1 | 2.0 |

## 5. Conclusions

The mechanical properties on the nanoscale of MCT-based heterostructures grown by molecular beam epitaxy on lattice mismatched GaAs (013) substrates with ZnTe/CdTe buffer layers, and epitaxial layers grown by liquid phase epitaxy on lattice matched CdZnTe (111) single crystal substrates, were studied by nanoindentation firstly and revealed possible phase transformations in MCT layers.

The pronounced "pop-out" effect caused, as a rule, by phase transformations in the materials tested was observed for the first time in lattice matched MCT layers in CdHgTe/CdZnTe heterostructures. In the lattice mismatched MBE-grown MCT-based heterostructures, the changes in the slopes of the unloading curves were observed which also testify to the presence of possible phase transformations in MCT layers.

The values of nanohardness and Young's modulus were obtained from the force-depth curves.

1. *Rogalski A.* Infrared Detectors. — Amsterdam: Gordon and Breach, 2000.
2. *De Lyon T. J., Jensen J. E., Gorwitz M. D. et al.* // J. Electr. Mater. — 1999. — **28.** — P. 705—707.
3. *Reine M. B.* // Proc. SPIE. — 2001. — **4288.** — P. 266—277.
4. *Varavin V. S., Dvoretsky S. A., Liberman V. I. et al.* // J. Cryst. Growth. — 1996. — **159.** — P. 1161—1167.
5. *Jim-Sang Kim, Se-Yonng An, Sang-Hee Suh*// Proc. SPIE. — 2002. — **4795.** — P. 207—212.
6. *Vasilyev V. V., Klimenko A. G., Marchishin I. V.et al.* // Infrared Phys. and Technology. — 2004. — **44.** — P. 13—23.

7. *Varavin V. S., Vasiliev V. V., Dvoretsky S. A. et al.* // Opto-Electronics Review. — 2003. — **11**. — P. 99—111.
8. *Qadri S. B., Skelton E. F., Webb A. W.* // J. Vac. Sci. Technol. — 1986. — **A4**. — P. 1974—1976.
9. *Martinez-Garcia D., Le Godec Y., Mezouar M. et al.* // Phys. status solidi (b). — 1999. — **211**. — P. 461—467.
10. *Nelmes R. J., McMahon M. I., Wright N. G. et al.* // Phys. Rev. Lett. — 1994. — **73**. — P. 1805—1808.
11. *McMahon M. I., Wright N. G., Allan D. R. et al.* // Phys. Rev. B. — 1996. — **53**. — P. 2163—2166.
12. *Nelmes R. J., McMahon M. I., Wright N. G. et al.* // Ibid. — 1995. — **51**. — P. 15723—15731.
13. *McMahon M. I., Nelmes R. J., Lin H. et al.* // Phys. Rev. Lett. — 1996. — **77**. — P. 1781—1784.
14. *Oliver W. C., Pharr G. M.* // J. Mater. Res. — 1992. — **7**. — P. 1562—1566.
15. *Timp G. L.* Nanotechnology. — New York: Springer, 1999.
16. *Chrisopher D., Smith R., Richter A.* // Nanotechnology. — 2001. — **12**. — P. 372—383.
17. *Domnich V., Gogotski Y.* // Rev. Adv. Mater. Sci. — 2002. — **3**. — P.1—36.
18. *Pang M., Bahr D. F., Lynn K. G.* // Appl. Phys. Lett. — 2003. — **82**. — P. 1200—1202.
19. *Wolf B., Swain M., Kempt M. et al.* // J. Mater. Sci. — 2000. — **35**. — P. 723—727.
20. *Osadchii V. M., Suslyakov A. O., Vasilyev V. V. et al.* // Fiz. Techn. Polupr. — 1999. — **33**. — P. 293—298 [Semiconductors. — 1999. — **33**, N3].
21. *Qadri S.B., Skelton E.F., Webb A.W.* // J. Vac. Sci. Technol. — 1986. — **A4**, N4. — P. 1971—1973.

Received 29.03.04

## ІНДУКОВАНІ НАНОІНДЕНТУВАННЯМ ФАЗОВІ ПЕРЕХОДИ В ЕПІТАКСІЙНИХ ГЕТЕРОСТРУКТУРАХ HgCdTe

*Ф. Сизов, А. Ріхтер, Є. Білевич, З. Цибрій, К. Кубіца, Р. Ріс, Ю. Сідоров*

Р е з ю м е

Епітаксійні гетероструктури кадмій—ртуть—телур (КРТ), вирощені методами молекулярно-променевої епітаксії (МПЕ) та рідкофазної епітаксії (РФЕ), були досліджені методом наноіндентування для виявлення можливих фазових переходів поблизу гетеромежі. Криві навантаження—зміщення при наноіндентуванні гетероструктур на основі КРТ, вирощених методом МПЕ на підкладках GaAs з буферним шаром ZnTe/CdTe, показали характерну "ліктеподібну" поведінку ділянок кривих за відсутності навантаження. У гетероструктурах КРТ, вирощених методом РФЕ на підкладках ZnCdTe, чіткіше виражений згин на аналогічних кривих та навіть спостерігається розрив залежностей, який в обох випадках (МПЕ та РФЕ), ймовірно, пов'язаний із структурними фазовими переходами поблизу гетеромежі.